Materials Research Bulletin 61 (2014) 326–332

Contents lists available at ScienceDirect

Materials Research Bulletin

journal homepage: www.elsevier.com/locate/matresbu

Effects of thiourea concentration on electrocatalytic performances of nickel sulfide counter electrodes for use in dye-sensitized solar cells

Yaoming Xiao *, Chenlu Wang, Gaoyi Han *

Institute of Molecular Science, Shanxi University, Taiyuan 030006, PR China

ARTICLE INFO

Article history:
Received 7 July 2014
Received in revised form 13 October 2014
Accepted 17 October 2014
Available online 18 October 2014

Keywords:
Inorganic compounds
Catalytic properties
Electrochemical techniques
Electrochemical measurements

ABSTRACT

The low-cost nickel sulfide counter electrode (NiS CE) for the dye-sensitized solar cell (DSSC) is electrodeposited onto the fluorinated tin oxide (FTO) glass substrate by using a cyclic voltammetry (CV) approach. The influences on the morphology and electrocatalytic performances of the NiS CE are studied by changing the thiourea concentration and the cycles of the CV electrodeposition. The electrochemical impedances and photoelectric performances of various DSSCs are also investigated. The results show that the preparation conditions for the best electrocatalytic performance of the NiS CE are under 1.00 mol L^{-1} of the thiourea concentration and 10 cycles of the CV electrodeposition, and the DSSC shows a photovoltaic conversion efficiency of 5.75% under full sunlight illumination (100 mW cm^{-2}, AM 1.5 G).

1. Introduction

Since the first report of the dye-sensitized solar cell (DSSC) in 1991, it has attracted extensive attentions due to its simple production process, low cost, and relatively high energy conversion efficiency [1–8]. The DSSC is usually composed of the dye-sensitized photoanode, I^-/I_3^-redox electrolyte, and counter electrode (CE). Typically, the CE applies a transparent F-doped tin oxide (FTO) or indium tin oxide (ITO) glass coated with platinum (Pt) nanoparticles. Pt acts as a good catalyst to speed up the reduction of I_3^- to I^- [1]. In spite of Pt having high electrocatalytic activity, it is not conducive to prepare large-scale of DSSCs due to its high cost and limited resource [6].

Numerous studies have been made with the aim of displacing the noble Pt by new materials in the DSSC, such as, metal catalytic materials [9–11], carbon-based materials [12–14], conducting polymers [15–20], and inorganic compounds [21–26]. Among them, nickel (Ni) has attracted much attentions due to its abundant resource, high electrical conductivity, and excellent electrochemical properties. Joshi et al. [10] incorporated Ni into carbon nanotubes/nanofibers on the FTO glass as the DSSC CE by using a thermal decomposition process. Bajpai et al. [11] prepared a Pt-free CE by coating Ni nanoparticles onto the graphene, the results showed that Ni nanoparticles could enhance the conductivity and catalytic ability of the CE. However, Ni could be reacted in the I^-/I_3^- redox couple electrolyte, which would bring about a negative effect on the long-term stability of the DSSC. The metal sulfide (MS, M=Ni, Co, Cu, Mo, W, etc.) is a class of effective catalytic material for the I_3^- reduction reaction in DSSCs, and the main methods for the MS preparation include electrochemical deposition [23], chemical bath deposition [27], and electrostatic self-assembly methods [28,29]. Guai et al. [30] electrophoretic deposited S-doped nickel oxide CEs, and obtained a DSSC efficiency of 5.04%. Dou et al. [31] reported a nickel phosphide-embedded graphene CE prepared by the hydrothermal reaction, and received 5.70% of the DSSC efficiency. Sun et al. [23] employed nickel sulfide (NiS) as the DSSC CE by a potential reversal technique, and the achieved DSSC efficiency of 6.83% was very close to that of the Pt CE (7%). Ku et al. [32] used NiS as the CE for the thiolate/disulfide mediated DSSC by a facile periodic potential reversal technique, gained an efficiency of 6.25% against that of 3.98% based on a Pt CE.

In this paper, we electrodeposited NiS CE onto the FTO glass by using a cyclic voltammetry (CV) approach, and investigated the influences of the thiourea concentration and the cycles of the CV electrodeposition on the morphology and electrocatalytic performances of the NiS CE. Under the optimum conditions, the DSSC obtained a photovoltaic conversion efficiency of 5.75% under full sunlight illumination (100 mW cm^{-2}, AM 1.5 G).

2. Experimental

2.1. Materials

Nickel chloride, thiourea, ethanol, iodine, lithium iodide, lithium pechlorate, tetrabutyl ammonium iodide, 4-*tert*-butyl-pyridine, and

* Corresponding authors. Tel.: +86 351 7010699; fax: +86 351 7016358.
E-mail addresses: ymxiao@sxu.edu.cn, ymxiao2011@sohu.com (Y. Xiao), han_gaoyis@sxu.edu.cn (G. Han).

http://dx.doi.org/10.1016/j.materresbull.2014.10.052
0025-5408/

acetonitrile were purchased from Shanghai Chemical Agent Ltd., China (analysis purity grade). Sensitized-dye N719 [*cis*-di(thiocyanato)-*N*,*N*′-bis(2,2′-bipyridyl-4-carboxylic acid-4-tetrabutylammonium carboxylate)ruthenium(II)] was purchased from Dyesol, Australia. The above agents were used without further purification. Fluorinated tin oxide (FTO) glass substrates were purchased from NSG, Japan ($8\,\Omega\,sq^{-1}$).

2.2. ***Electrodeposition of*** *NiS CEs*

Prior to the electrodeposition, FTO glass substrates (1.5 cm × 2 cm) were cleaned with deionized water and ethanol in sequence. Three kinds of different electrodeposition solutions were prepared by containing same concentration of nickel chloride ($0.05\,mol\,L^{-1}$) and adding different concentrations of thiourea ($0.75\,mol\,L^{-1}$, $1.0\,mol\,L^{-1}$, and $1.25\,mol\,L^{-1}$, respectively). The CV electro deposition of NiS thin film onto FTO glass substrates were carried out using a computer-controlled Autolab potentiostat (Type III) from an aforementioned electrodeposition solution in a three compartment cell at ambient atmosphere. A cleaned FTO glass substrate, a saturated silver/silver chloride (Ag/AgCl), and a Pt wire were used as the working electrode, the reference electrode, and the counter electrode, respectively. The parameters for NiS CEs were set under the potential interval ranging from −0.9 V to 0.7 V at a scan rate of $0.05\,V\,s^{-1}$ for 5, 10, and 15 cycles, respectively. The achieved NiS CEs were washed in distilled water and dried under a cool air flow. The parameters and sample names for the NiS CEs were listed in Table 1. For comparison, a thermal decomposition Pt CE was employed.

2.3. Assembly of DSSCs

The TiO_2 photoanodes were prepared according to our previous reports [2,5]. The resultant TiO_2 photoanodes were further sensitized by immersing them into a $0.25\,mmol\,L^{-1}$ ethanolic solution of N719 dye for 24 h, followed by air drying. After dye adsorption, the TiO_2 photoanodes were assembled with various CEs. Then the electrolyte was injected into the cell. The redox electrolyte, composed of $0.60\,mol\,L^{-1}$ tetrabutyl ammonium iodide, $0.10\,mol\,L^{-1}$ lithium iodide, $0.10\,mol\,L^{-1}$ iodine, and $0.50\,mol\,L^{-1}$ 4-*tert*-butyl-pyridine in acetonitrile, was employed in photovoltaic conversion measurements.

2.4. Characterizations and measurements

The surface features of the NiS CEs were observed using a scanning electron microscopy (SEM, JEOL-JSM-6701F) operating at 10 kV. The phase identification of the NiS CE was conducted with powder X-ray diffraction (XRD, BRUKER D8-ADVANCE). CVs for I^-/I_3^- system were measured in an acetonitrile solution consisting of $0.05\,mol\,L^{-1}$ lithium iodide, $0.01\,mol\,L^{-1}$ iodine, and $0.05\,mol\,L^{-1}$ lithium pechlorate, the potential window was −0.8 V to 1.2 V (vs. Pt) with different scan rates (50, 75, 100, and $125\,mV\,s^{-1}$) using a computer-controlled potentiostat (Autolab Type III) in a three-electrode electro-chemical cell at a constant temperature of 15 °C, the resultant CEs acted as the working electrode, a Pt-foil as counter electrode and a Pt-wire as reference electrode. The electrochemical impedance spectroscopy (EIS) measurements for the DSSCs were conducted by using an electrochemical work station system (CHI660D, Shanghai Chenhua Device Company, China) at a constant temperature of 15 °C in ambient atmosphere under a dark condition, and the impedance data covered a frequency range of $1–10^5$ Hz with 5 mV of amplitude and 0.8 V bias potential. The resultant impedance spectra were analyzed by means of the Z-view software. The photocurrent density–voltage characteristic of the DSSC was carried out using a computer-controlled CHI660D under illumination by a solar simulator (CEL-S500, Beijing Ceaulight Science and Technology Ltd., China) in ambient atmosphere. The active cell area and the incident light intensity were $0.30\,cm^2$ and $100\,mW\,cm^{-2}$ (AM 1.5 G), respectively. The photoelectronic performances [i.e., fill factor (FF) and overall energy conversion efficiency (η)] were calculated by the following equations [33]:

$$FF = \frac{V_{max} \times J_{max}}{V_{oc} \times J_{sc}} \quad (1)$$

$$\eta(\%) = \frac{V_{max} \times J_{max}}{P_{in}} \times 100\% = \frac{V_{oc} \times J_{sc} \times FF}{P_{in}} \times 100\% \quad (2)$$

where J_{SC} is the short-circuit current density ($mA\,cm^{-2}$), V_{OC} is the open-circuit voltage (V), P_{in} is the incident light power, J_{max} ($mA\,cm^{-2}$), and V_{max} (V) are the current density and voltage in the *J*–*V* curves at the point of maximum power output, respectively.

Table 1
The preparation parameters of various NiS CEs.

CE	Thiourea concentration ($mol\,L^{-1}$)	CV cycles
NiS-a	0.75	10
NiS-b	1.00	10
NiS-c	1.25	10
NiS-d	1.00	5
NiS-e	1.00	15

3. Results and discussion

3.1. Composition of the NiS CE

XRD pattern was employed to investigate the composition of the NiS attached on the FTO glass substrate. In Fig. 1, the crystalline phase of NiS-b can be observed at 30.2, 34.8, 46.0, 53.7, and 73.0°, which are identified to be the (1 0 0), (1 0 1), (1 0 2), (1 1 0), and (2 0 2) diffraction signals, respectively, according to the Joint Committee on Powder Diffraction Standards (JCPDS card No. 75-0613) [34]. And other strong peaks are corresponding to the bare FTO glass. XRD patterns for other NiS CEs are the same as those of the NiS-b, this indicates that the NiS-based CE was successfully electrodeposited onto the FTO glass.

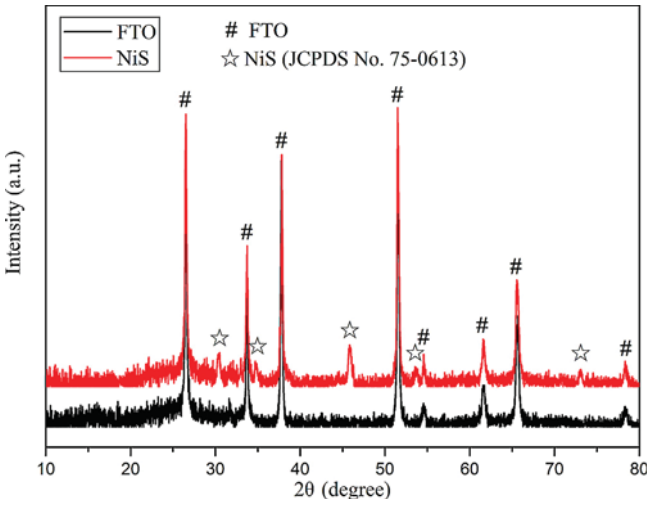

Fig. 1. XRD patterns of the bare FTO and NiS-b CE.

3.2. Morphology of the NiS CE

Fig. 2 shows the SEM images of the NiS CEs prepared by different electrodeposition conditions. Fig. 2a–c shows that the morphologies of various NiS CEs were observably influenced by the thiourea concentration. The NiS nanoparticle is very tiny under the low thiourea concentration of 0.75 mol L^{-1} (Fig. 2a). The NiS nanoparticles become larger when increasing the thiourea concentration to 1.00 mol L^{-1} (Fig. 2b), this is due to the high thiourea concentration which could improve the deposition rate of the NiS growth. In other words, the higher the thiourea concentration, the more thiourea is available to the electrode surface from the bulk solution to support the NiS electrodeposition. However, some inconsecutive voids appeared in the NiS film under the thiourea concentration of 1.25 mol L^{-1} (Fig. 2c), this is owing to that, the excessive thiourea concentration might tremendously increase the deposition rate, resulting in the unequally electrochemical deposition process. Therefore, the best thiourea concentration for the opportune size of the NiS CE is 1.00 mol L^{-1}. According to Fig. 2b,d, and e, adding CV cycles would lead to larger NiS nanoparticles. From 5 to 10 CV cycles, the range of NiS increase is not obvious, but from 10 to 15 CV cycles, the NiS nanoparticles increase is obvious. An opportune size of the NiS nanoparticles can support a high surface area of the NiS CE, which is benefit for enhancing the electrocatalytic activity of the NiS CE.

3.3. Electrocatalytic activities of the NiS CE

CV measurements were carried out to study the catalytic performances of the NiS CEs in the I^-/I_3^- system, and a thermal decomposition Pt CE was used as the reference for comparison. As shown in Fig. 3, all CEs show two pairs of oxidation and reduction peaks, the redox pair on the left is owing to the redox reaction of $I_3^- + 2e^- \leftrightarrow 3I^-$, which directly affects the performance of the DSSC; while that on the right is due to the redox reaction of $3I_2 + 2e^- \leftrightarrow 2I_3^-$, which has little effect on the DSSC performance [5,35]. The Pt catalyst has the highest peak current density among all the CEs. The NiS-b CE is the best one among all the NiS-based CEs,

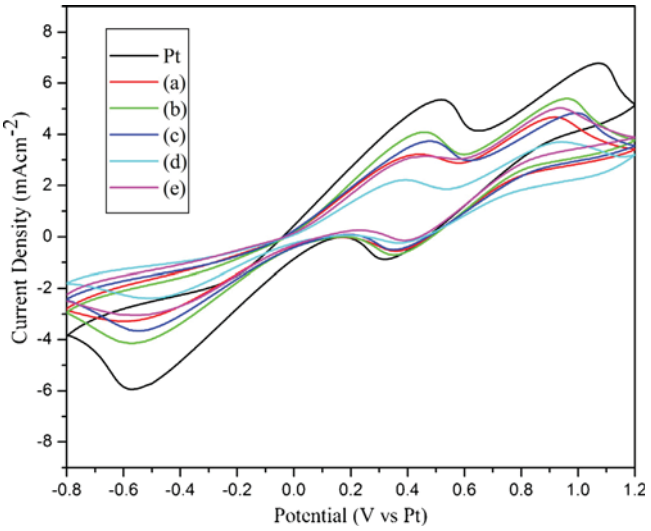

Fig. 3. CVs of the (Pt) Pt, (a) NiS-a, (b) NiS-b, (c) NiS-c, (d) NiS-d, and (e) NiS-e CEs, respectively.

suggesting that the NiS-b CE has the highest electrocatalytic activity compared to NiS-based CEs, which can be attributed to its opportune size of NiS nanoparticles with the largest active surface area, as discussed in the subsequent EIS results.

Fig. 4 shows CVs of the I_3^-/I^- system on the Pt and various NiS CEs at different scan rates. For all the CEs, the anodic peaks regularly and gradually shifted positively, and the corresponding cathodic peaks also shifted negatively while increasing the scan rate. Fig. 5 shows a linear relationship between the anodic (or cathodic) peak current density and the square root of the scan rate, illustrating that this redox reaction is diffusion limited at either the Pt CE or NiS-based CEs, which may be attributed to the diffusion of iodide species off of the CE surface [36,37]. Moreover, the diffusion coefficient (D_n) in the Randles–Sevcik equation ($J_{red} = Kn^{1.5}AC(D_n)^{0.5}\nu^{0.5}$) can be calculated from the correlation between the

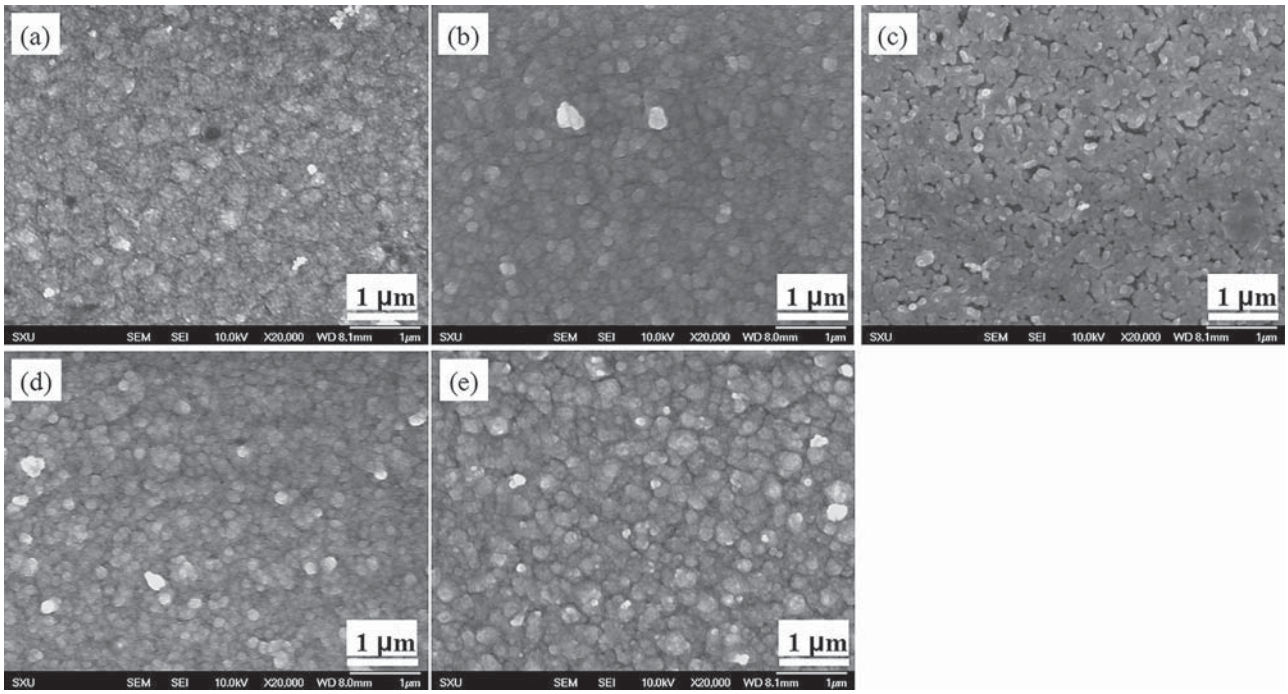

Fig. 2. SEM images of the (a) NiS-a, (b) NiS-b, (c) NiS-c, (d) NiS-d, and (e) NiS-e CEs, respectively.

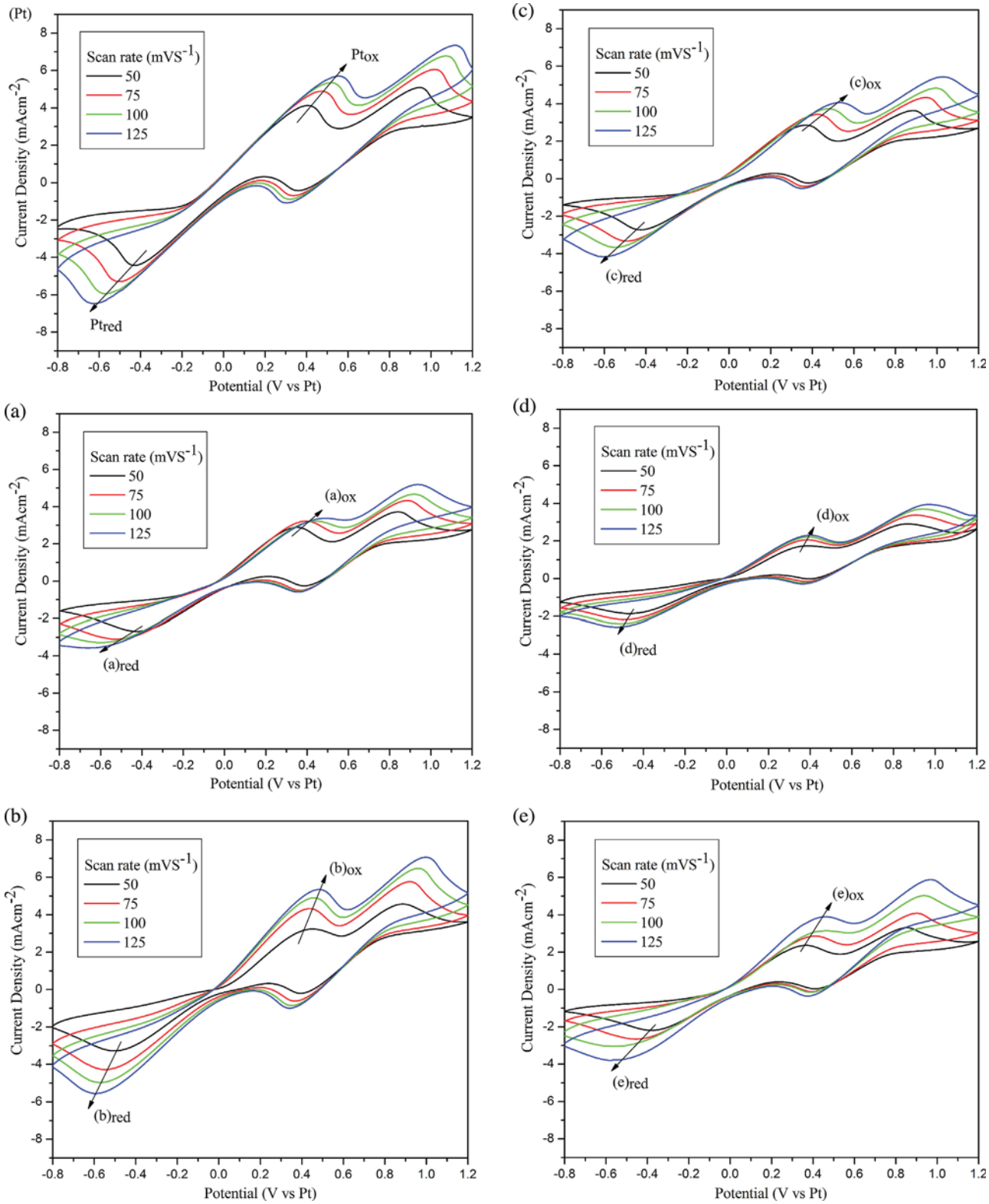

Fig. 4. CVs of the (Pt) Pt, (a) NiS-a, (b) NiS-b, (c) NiS-c, (d) NiS-d, and (e) NiS-e CEs at different scan rates (from inner to outer: 50, 75, 100, and 125 mV s^{-1}, respectively), respectively.

peak current density (J_{red}) and scan rate (v). Where K represents the constant of 2.69×10^5, n stands for the number of electrodes devoting to the charge transfer, A is the electrode area, and C is the bulk concentration of I_3^- species. As listed in Table 3, the Pt CE shows the highest D_n of 5.31×10^{-6} cm^{-2} s^{-1}, demonstrating it has the best catalytic performance [36–38]. The NiS-b CE has the largest D_n of 3.65×10^{-6} cm^{-2} s^{-1} among all of the NiS-based CEs, implying it has a highest electrocatalytic activity compared to the NiS-based CEs. These results are in accordance with those of in Figs. 2 and 3 .

Furthermore, Fig. 6a shows consecutive CV measurements of the NiS-b CE, the peak positions and peak current densities both

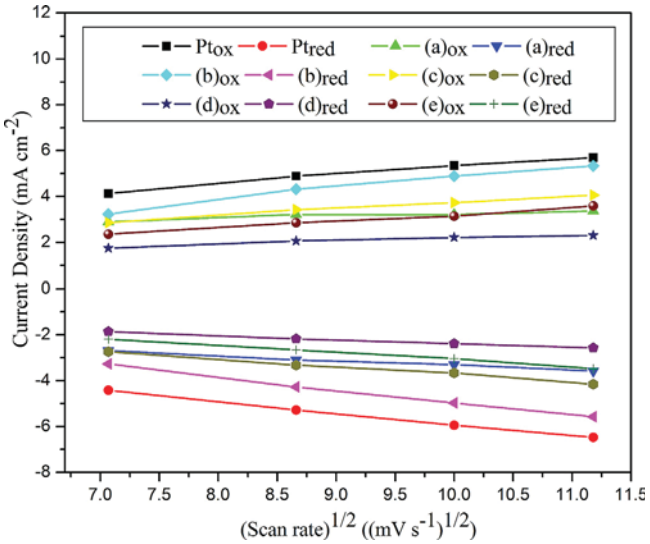

Fig. 5. Relationships between all the redox peak currents and scan rates in Fig. 4.

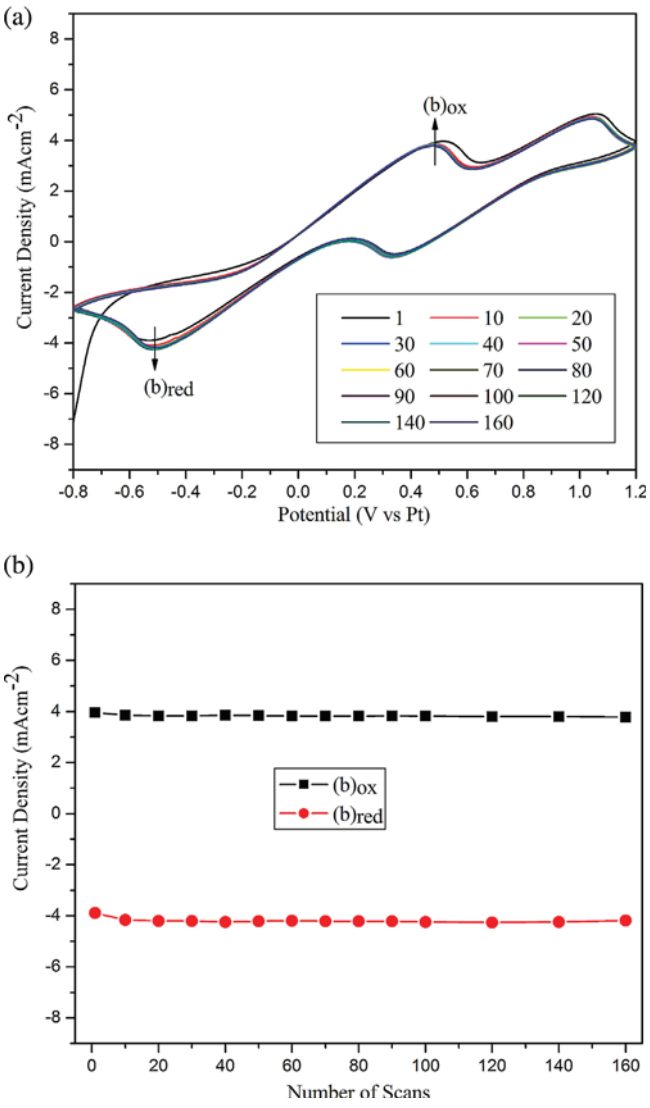

Fig. 6. Consecutive 160CVs (a) of I^-/I_3^- system for NiS-b CE at a scan rate of 100 mV s^{-1}, the relationship (b) between the number of scans and the resultant redox peak currents from Fig. 6a.

have a little change. The correlations between the peak current densities and the number of scans were summarized in Fig. 6b. Both redox peak current densities retain stable with increasing the number of scan. This proves that the NiS-b CE is tightly bound to the FTO glass surface and has good chemical stability [39].

3.4. Electrochemical impedance and photovoltaic performance of the DSSC

The electrochemical impedance spectroscopy (EIS) for the DSSC was shown in Fig. 7. The equivalent circuit of this model (inset of Fig. 7) has been already reported [40]. The results of the fitted impedance data are shown in Table 2. The intercept of the real axis at high frequency refers to the ohmic series resistance (R_S) containing the sheet resistance of the anode, the counter electrode, and the electrolytic. The first semicircle at high frequency represents the R_{CT}(CE), which is an important correlation with the electrocatalytic activity of the CE, the lower R_{CT}(CE), the higher catalytic performance of the CE. While the second semicircle at middle frequency is the $R_{CT}(TiO_2)$ for the charge-transfer resistance at the electrolyte/anode interface [41], and the third semicircle at low frequency stands for the Nernst diffusion impedance (W) on the diffusion resistance of the I^-/I_3^- redox species. The constant phase elements (Y_{CPE}(CE) and $Y_{CPE}(TiO_2)$) are frequently used as substitutes for the capacitors in an equivalent circuit to fit the impedance behavior while the electrical double layer does not behave as an ideal capacitor [41]. Comparing to the R_S values of the NiS-based CEs, the slight change is attributed to the different morphology size of the NiS caused by different preparation conditions. However, the R_{CT}(CE) value (9.48 Ω cm^2) of the NiS-b CE is the smallest one among all the NiS-based CEs, indicating it has the highest electrocatalytic activity compared to the NiS-based CEs. The lower R_{CT}(CE), the higher fill factor (FF) and the higher cell efficiency (η) [36,42,43]. In addition, a larger Y_{CPE}(CE) of the CE corresponds to its larger surface area. The highest Y_{CPE}(CE) value of the NiS-b CE (0.94 mF cm^{-2}) shows its largest surface area, which can enhance the electrocatalytic activity. These results are in accordance with the results of the CV and SEM.

Fig. 8 shows the photovoltaic performances of DSSCs based on various CEs under full sunlight illumination (100 mW cm^{-2}, AM 1.5 G), which were reproduced many times without obvious change, and the resultant photovoltaic parameters were summarized in Table 3. It is obvious that the DSSC based on the Pt CE has

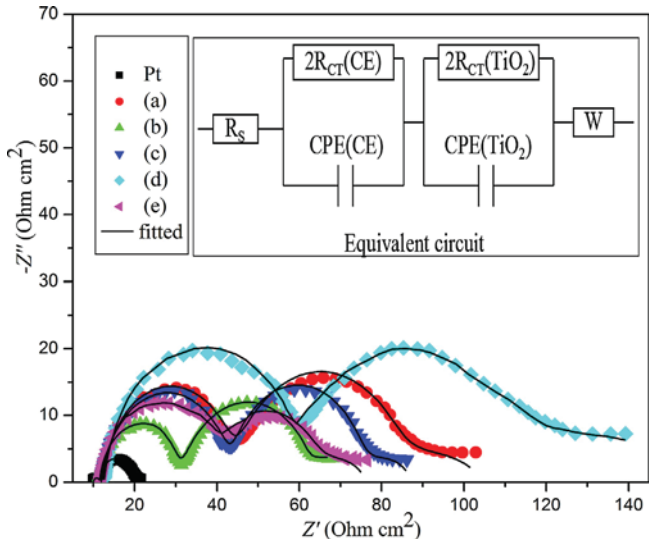

Fig. 7. Nyquist plots of the DSSCs based on the Pt, (a) NiS-a, (b) NiS-b, (c) NiS-c, (d) NiS-d, and (e) NiS-e CEs, respectively.

Table 2
Best-fit values for R_S,R_{CT}(CE), Y_{CPE}(CE), and W of the equivalent circuits to the EIS in Fig. 7.

CE	R_S (Ω cm^2)	R_{CT}(CE) (Ω cm^2)	Y_{CPE}(CE) (mF cm^{-2})	W (Ω cm^2)
Pt	9.97 ± 0.01	0.75 ± 0.01	0.85	2.38 ± 0.01
(a)	11.61 ± 0.02	15.81 ± 0.02	0.92	12.59 ± 0.02
(b)	11.76 ± 0.02	9.48 ± 0.01	0.94	7.26 ± 0.02
(c)	11.93 ± 0.03	15.63 ± 0.01	0.89	9.86 ± 0.01
(d)	12.09 ± 0.02	22.66 ± 0.02	0.75	15.76 ± 0.02
(e)	11.87 ± 0.02	13.41 ± 0.02	0.86	9.05 ± 0.02

Table 3
The photovoltaic parameters of DSSCs with Pt, (a) NiS-a, (b) NiS-b, (c) NiS-c, (d) NiS-d, and (e) NiS-e CEs, respectively.

CE	D_n (cm^{-2} s^{-1})	J_{SC} (mA cm^{-2})	V_{OC} (mV)	FF	η (%)
Pt	5.31×10^{-6}	16.76	750	0.62	7.79
(a)	7.75×10^{-7}	14.98	730	0.26	2.84
(b)	3.65×10^{-6}	16.68	734	0.47	5.75
(c)	1.98×10^{-6}	15.65	732	0.30	3.44
(d)	5.04×10^{-7}	14.82	730	0.25	2.70
(e)	2.45×10^{-6}	16.35	733	0.40	4.79

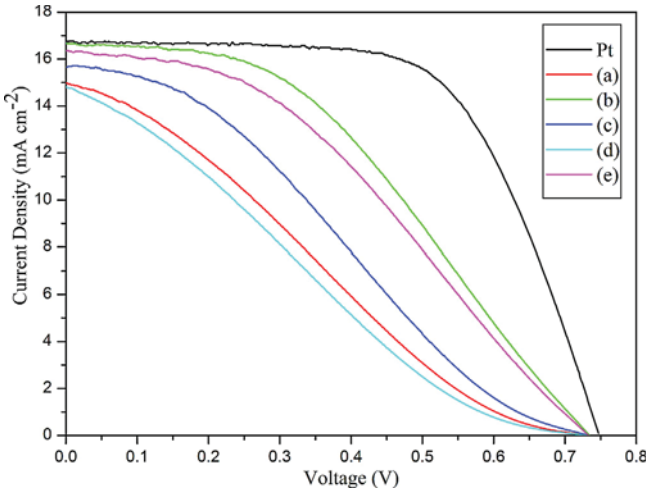

Fig. 8. Photocurrent density–voltage characteristics of DSSCs under 100 mW cm^{-2} (AM 1.5 G) based on the Pt, (a) NiS-a, (b) NiS-b, (c) NiS-c, (d) NiS-d, and (e) NiS-e CEs, respectively.

the best photovoltaic performances due to its highest electrocatalytic activity. Among all the NiS-based CEs, the DSSC with the NiS-b CE obtained the best η of 5.75%. As a result, the electrocatalytic activity of the CE would observably influence the the short-current density (J_{SC}) and FF of the DSSC, the higher electrocatalytic activity, the higher reaction rate of the I^-/I_3^- system, the lower electrochemical impedance, finally the higher J_{SC} and FF of the DSSC.

4. Conclusions

In summary, NiS CEs were fabricated by using a CV deposition method, the influences of the thiourea concentration and the CV cycles on the electrocatalytic and photoelectric performances of the NiS CE were investigated. The optimum conditions for the NiS-b CE were under 1.00 mol L^{-1} of the thiourea concentration and 10 cycles of the CV electrodeposition. The NiS-b CE showed a good chemical stability and high electrocatalytic activity with the D_n of 3.65×10^{-6} cm^{-2} s^{-1} for the I^-/I_3^- diffusion on its surface. The DSSC based on the NiS-b CE obtained a J_{SC} of 16.68 mA cm^{-2}, V_{OC} of 734 mV, FF of 0.47, and η of 5.75% under full sunlight illumination (100 mW cm^{-2}, AM 1.5 G).

Acknowledgments

The authors appreciate funding from National Natural Science Foundation of China (21274082) and Shanxi Province (2014011016-1), the Program for New Century Excellent Talents in University (NCET-10-0926), Scientific and Technologial Innovation Programs of Higher Education Institutions in Shanxi (020352901014), and the Scientific Research Start-up Funds of Shanxi University (020351801003).

References

[1] B. O'Regan, M. Grätzel, Low-cost high-efficiency solar cell based on dye-sensitized colloidal TiO_2 films, Nature 353 (1991) 737–740.
[2] J. Wu, Z. Lan, J. Lin, M. Huang, S. Hao, T. Sato, S. Yin, A novel thermosetting gel electrolyte for stable quasi-solid-state dye-sensitized solar cells, Adv. Mater. 19 (2007) 4006–4011.
[3] A. Yella, H. Lee, H. Tsao, C. Yi, A. Chandiran, M. Nazeeruddin, E. Diau, C. Yeh, S. Zakeeruddin, M. Grätzel, Porphyrin-sensitized solar cells with cobalt(II/III)-based redox electrolyte exceed 12 percent efficiency, Science 334 (2011) 629–634.
[4] L. Han, A. Islam, H. Chen, C. Malapaka, B. Chiranjeevi, S. Zhang, X. Yang, M. Yanagida, High-efficiency dye-sensitized solar cell with a novel co-adsorbent, Energy Environ. Sci. 5 (2012) 6057–6060.
[5] J. Wu, Y. Xiao, G. Yue, Q. Tang, J. Lin, M. Huang, Y. Huang, L. Fan, Z. Lan, S. Yin, T. Sato, A large-area light-weight dye-sensitized solar cell based on all titanium substrates with an efficiency of 6.69% outdoors, Adv. Mater. 24 (2012) 1884–1888.
[6] A. Hagfeldt, G. Boschloo, L. Sun, L. Kloo, H. Pettersson, Dye-sensitized solar cells, Chem. Rev. 110 (2010) 6595–6663.
[7] S. Mathew, A. Yella, P. Gao, R. Humphry-Baker, B. Curchod, N. Ashari-Astani, I. Tavernelli, U. Rothlisberger, M. Nazeeruddin, M. Grätzel, Dye-sensitized solar cells with 13% efficiency achieved through the molecular engineering of porphyrin sensitizers, Nat. Chem. 6 (2014) 242–247.
[8] S. Park, I. Chung, J. Woo, T. Kim, Z. Li, M. Jin, D. Lee, J. Kim, Improvement of dye-sensitized solar cell performance through infiltration of TiO_2 nanoparticles between mesoporous TiO_2 particles, Mater. Res. Bull. (2014) , doi:http://dx.doi.org/10.1016/j.materresbull.2014.04.062.
[9] E. Olsen, G. Hagen, S. Lindquist, Dissolution of platinum in methoxy propionitrile containing LiI/I_2, Sol. Energy Mater. Sol. Cells 63 (2000) 267–273.
[10] P. Joshi, Z. Zhou, P. Poudel, A. Thapa, X. Wu, Q. Qiao, Nickel incorporated carbon nanotube/nanofiber composites as counter electrodes for dye-sensitized solar cells, Nanoscale 4 (2012) 5659–5664.
[11] R. Bajpai, S. Roy, N. Kulshrestha, J. Rafiee, N. Koratkar, D. Misra, Graphene supported nickel nanoparticle as a viable replacement for platinum in dye sensitized solar cells, Nanoscale 4 (2012) 926–930.
[12] S. Huang, L. Li, Z. Yang, L. Zhang, H. Saiyin, T. Chen, H. Peng, A new and general fabrication of an aligned carbon nanotube/polymer film for electrode applications, Adv. Mater. 23 (2011) 4707–4710.
[13] T. Chen, L. Qiu, Z. Yang, Z. Cai, J. Ren, H. Li, H. Lin, X. Sun, H. Peng, An integrated energy wire for both photoelectric conversion and energy storage, Angew. Chem. Int. Ed. 51 (2012) 11977–11980.
[14] G. Wang, Y. Fang, Y. Lin, W. Xing, S. Zhuo, Nitrogen-doped graphene as transparent counter electrode for efficient dye-sensitized solar cells, Mater. Res. Bull. 47 (2012) 4252–4256.
[15] J. Wu, Q. Li, L. Fan, Z. Lan, J. Lin, P. Li, M. Huang, S. Hao, High-performance polypyrrole nanoparticles counter electrode for dye-sensitized solar cells, J. Power Sources 181 (2008) 172–176.
[16] Y. Xiao, J. Lin, S. Tai, S. Chou, G. Yue, J. Wu, Pulse electropolymerization of high performance PEDOT/MWCNT counter electrodes for Pt-free dye-sensitized solar cells, J. Mater. Chem. 22 (2012) 19919–19925.
[17] Y. Xiao, J. Lin, J. Wu, S. Tai, G. Yue, Dye-sensitized solar cells with high-performance PANI/MWCNT counter electrodes electropolymerized by a pulse potentiostatic technique, J. Power Sources 233 (2013) 320–325.
[18] Q. Tang, H. Cai, S. Yuan, X. Wang, Counter electrodes from double-layered polyaniline nanostructures for dye-sensitized solar cell applications, J. Mater. Chem. A 1 (2013) 317–323.
[19] J. Luo, H. Niu, H. Wen, W. Wu, P. Zhao, C. Wang, X. Bai, W. Wang, Enhancement of the efficiency of dye-sensitized solar cell with multi-wall carbon nanotubes/polypyrrole composite counter electrodes prepared by electrophoresis/electrochemical polymerization, Mater. Res. Bull. 48 (2013) 988–994.
[20] Y. Xiao, G. Han, Y. Li, M. Li, Y. Chang, High performance of Pt-free dye-sensitized solar cells based on two-step electropolymerized polyaniline counter electrodes, J. Mater. Chem. A 2 (2014) 3452–3460.
[21] G. Li, J. Song, G. Pan, X. Gao, Highly Pt-like electrocatalytic activity of transition metal nitrides for dye-sensitized solar cells, Energy Environ. Sci. 4 (2011) 1680–1683.

[22] M. Wu, Q. Zhang, J. Xiao, C. Ma, X. Lin, C. Miao, Y. He, Y. Gao, A. Hagfeldt, T. Ma, Two flexible counter electrodes based on molybdenum and tungsten nitrides for dye-sensitized solar cells, J. Mater. Chem. 21 (2011) 10761.
[23] H. Sun, D. Qin, S. Huang, X. Guo, D. Li, Y. Luo, Q. Meng, Dye-sensitized solar cells with NiS counter electrodes electrodeposited by a potential reversal technique, Energy Environ. Sci. 4 (2011) 2630–2637.
[24] Y. Xiao, J. Wu, J. Lin, S. Tai, G. Yue, Pulse electrodeposition of CoS on the MWCNT/Ti as a high performance counter electrode for the Pt-free dye-sensitized solar cell, J. Mater. Chem. A 1 (2013) 1289–1295.
[25] Y. Xiao, J. Wu, J. Lin, G. Yue, J. Lin, M. Huang, Y. Huang, Z. Lan, L. Fan, A high performance Pt-free counter electrode of nickel sulfide/multiwall carbon nanotubes/titanium used in dye-sensitized solar cells, J. Mater. Chem. A 1 (2013) 13885–13889.
[26] F. Gong, H. Wang, X. Xu, G. Zhou, Z. Wang, In situ growth of $Co_{0.85}Se$ and $Ni_{0.85}Se$ on conductive substrates as high-performance counter electrodes for dye-sensitized solar cells, J. Am. Chem. Soc. 134 (2012) 10953–10958.
[27] C. Kung, H. Chen, C. Lin, K. Huang, R. Vittal, K. Ho, CoS acicular nanorod arrays for the counter electrode of an efficient dye-sensitized solar cell, ACS Nano 6 (2012) 7016–7025.
[28] W. Chi, J. Han, S. Yang, D. Roh, H. Lee, J. Kim, Employing electrostatic self-assembly of tailored nickel sulfide nanoparticles for quasi-solid-state dye-sensitized solar cells with Pt-free counter electrodes, Chem. Commun. 48 (2012) 9501–9503.
[29] H. Mulmudi, S. Batabyal, M. Rao, R. Prabhakar, N. Mathews, Y. Lam, S. Mhaisalkar, Solution processed transition metal sulfides: application as counter electrodes in dye sensitized solar cells (DSCs), Phys. Chem. Chem. Phys. 13 (2011) 19307–19309.
[30] G. Guai, M. Leiw, C. Ng, C. Li, Sulfur-doped nickel oxide thin film as an alternative to Pt for dye-sensitized solar cell counter electrodes, Adv. Energy Mater. 2 (2012) 334–338.
[31] Y. Dou, G. Li, J. Song, X. Gao, Nickel phosphide-embedded graphene as counter electrode for dye-sensitized solar cells, Phys. Chem. Chem. Phys. 14 (2012) 1339–1342.
[32] Z. Ku, X. Li, G. Liu, H. Wang, Y. Rong, M. Xu, L. Liu, M. Hu, Y. Yang, H. Han, Transparent NiS counter electrodes for thiolate/disulfide mediated dye-sensitized solar cells, J. Mater. Chem. A 1 (2013) 237–240.
[33] M. Grätzel, Perspectives for dye-sensitized nanocrystalline solar cells, Prog. Photovoltaic Res. Appl. 8 (2000) 171–185.
[34] H. Bi, W. Zhao, S. Sun, H. Cui, T. Lin, F. Huang, X. Xie, M. Jiang, Graphene films decorated with metal sulfide nanoparticles for use as counter electrodes of dye-sensitized solar cells, Carbon 61 (2013) 116–123.
[35] Y. Xiao, J. Wu, G. Yue, J. Lin, M. Huang, Z. Lan, Low temperature preparation of a high performance Pt/SWCNT counter electrode for flexible dye-sensitized solar cells, Electrochim. Acta 56 (2011) 8545–8550.
[36] Y. Saito, W. Kubo, T. Kitamura, Y. Wada, S. Yanagida, I^-/I_3^- redox reaction behavior on poly(3,4-ethylenedioxythiophene) counter electrode in dye-sensitized solar cells, J. Photochem. Photobiol. A 164 (2004) 153–157.
[37] S. Biallozor, A. Kupniewska, Study on poly(3,4-ethylenedioxythiophene) behaviour in the I^-/I_2 solution, Electrochem. Commun. 2 (2000) 480–486.
[38] J. Lin, J. Liao, Mesoporous electrodeposited-CoS film as a counter electrode catalyst in dye-sensitized solar cells, J. Electrochem. Soc. 159 (2012) D65–D71.
[39] H. Guo, Y. Li, L. Fan, X. Wu, M. Guo, Voltammetric behavior study of folic acid at phosphomolybdic-polypyrrole film modified electrode, Electrochim. Acta 51 (2006) 6230–6237.
[40] H. Wang, F. Wang, Y. Wang, C. Wan, B. Hwang, R. Santhanam, J. Rick, Electrochemical formation of Pt nanoparticles on multiwalled carbon nanotubes: useful for fabricating electrodes for use in dye-sensitized solar cells, J. Phys. Chem. C 115 (2011) 8439–8446.
[41] Y. Zheng, X. Tao, L. Wang, H. Xu, Q. Hou, W. Zhou, J. Chen, Novel ZnO-based film with double light-scattering layers as photoelectrodes for enhanced efficiency in dye-sensitized solar cells, Chem. Mater. 22 (2010) 928–934.
[42] G. Mor, K. Shankar, M. Paulose, O. Varghese, C. Grimes, Use of highly-ordered TiO_2 nanotube arrays in dye-sensitized solar cells, Nano Lett. 6 (2006) 215–218.
[43] E. Ramasamy, W. Lee, D. Lee, J. Song, Parallel grid dye-sensitized solar cell module prepared by screen printing, J. Power Sources 165 (2007) 446–449.